Anomaly in the nuclear charge radii of Zr isotopes

M. Hemalatha,[1,*] A. Bhagwat,[2] A. Shrivastava,[1] S. Kailas,[1] and Y. K. Gambhir[2]
[1]*Nuclear Physics Division, Bhabha Atomic Research Centre, Mumbai 400 085, India*
[2]*Department of Physics, IIT-Powai, Mumbai 400 076, India*
(Received 2 April 2004; published 29 October 2004)

The recent laser spectroscopic measurements of nuclear root-mean-square charge radii on a chain of Zr isotopes exhibit a rich structure. A prominent kink is observed at ^{90}Zr and a sharp change is noticed between ^{98}Zr and ^{100}Zr, in the neutron rich region. In the present work, the ground state properties of these nuclei are calculated in the relativistic mean field (RMF) framework. The calculations are in good accord with the experiment. The RMF densities are folded with the extended Jeukenne, Lejeune, and Mahaux energy and density dependent nucleon-nucleon interaction to yield the semimicroscopic optical potential which in turn is used to calculate the elastic scattering cross sections for 50 MeV proton scattering from a chain of Zr isotopes. The differential cross sections obtained from the calculations agree remarkably well with the experiment. The calculation reveals a correlation between the mean-square charge radii and the corresponding reaction cross sections for $A \geqslant 88$. There is a monotonic increase in σ_R from $A=84$ to 106 with the hint of a slight jump from $A=98$ to $A=100$.

DOI: 10.1103/PhysRevC.70.044320 PACS number(s): 21.10.−k, 21.60.−n, 24.10.−i, 25.40.Cm

I. INTRODUCTION

The recent laser spectroscopic measurements of nuclear root-mean-square (rms) charge radii ($\langle r_c \rangle$) on a chain of zirconium isotopes [1] exhibit remarkable features. It is observed that the $\langle r_c \rangle$ values increase with the addition of neutrons. There appears a sudden jump in the $\langle r_c \rangle$ values while going from ^{98}Zr to ^{100}Zr in the neutron rich region. Further, a kink is observed at $N=50$ (^{90}Zr). Removal of two neutrons from $N=50$ slightly increases $\langle r_c \rangle$, instead of the decrease expected from the conventional $r_0 A^{1/3}$ relation. This is termed as an anomalous behavior. Similar anomalous behavior has been observed [2,3] for several isotopic chains throughout the periodic table. The analysis of initial experiments with the radioactive ion beams (RIB) led Tanihata *et al.* [4] to associate sudden jumps in the observed reaction cross sections with the addition of neutrons to the corresponding sudden increase in the matter radius of the projectile. For example, a sudden jump in the reaction cross section observed while going from ^{9}Li to ^{11}Li had been associated with a large increase in the matter radius of ^{11}Li with the addition of two neutrons. Based on this observation, it is expected that one may observe a similar jump in the reaction cross section (though may be less pronounced) while going from ^{98}Zr to ^{100}Zr. The *p*-Zr elastic scattering data are available for the stable Zr ($A=90$–$A=96$) isotopes [5]. However, the cross section data for ^{98}Zr and ^{100}Zr are not available. In the present work, we have predicted the reaction cross sections for p-$^{78-106}$Zr systems to investigate the correlation between the charge radii values and the reaction cross sections. With the present day available RIB facilities, it should be possible to perform elastic scattering experiments using proton as target and the Zr isotopes as projectiles to verify these theoretical predictions.

The calculations presented here proceed in three steps. In the first step, the ground state properties of the Zr isotopes are calculated in the relativistic mean field (RMF) [6] framework. The calculated binding energies, the quadrupole deformation parameters, the one and two neutron separation energies, the neutron and the charge radii, etc., compare well with the experiment (where available). In the next step, the calculated RMF densities are employed in the semimicroscopic optical model to determine the proton optical potentials for the different Zr isotopes. For this purpose, the densities are folded with the extended Jeukenne, Lejeune, and Mahaux (JLM) energy and density dependent nucleon-nucleon interaction using the computer code MOM (microscopic optical model) [7]. This yields both the real and imaginary parts of the respective optical potentials. In the final step, this optical potential (both the real and imaginary parts) is used to compute the reaction and the differential cross sections for 50 MeV proton scattering from the even mass number Zr isotopes, both stable and unstable.

The essentials of RMF formulation required in the calculation of the ground state properties are contained in Sec. II. The RMF results for Zr isotopes are presented and discussed in the same section. Section III is devoted to the calculation of the optical potential. In Sec. IV the differential cross sections and the reaction cross section calculations for 50 MeV *p* scattering from even Zr isotopes and comparison with the experimental data (where available) are presented.

II. ESSENTIALS OF RMF

The present version of the RMF theory, essentially based on the Walecka model [8] starts with a Lagrangian describing the Dirac spinor nucleons interacting via the electromagnetic (e.m.) and meson fields. The scalar sigma (σ), vector omega (ω), and iso-vector vector rho (ρ) mesons are considered. The Lagrangian consists of free baryon and meson terms and the interaction terms. The variational principle yields the

*Electronic address: mhema@magnum.barc.ernet.in

equations of motion. Replacing the fields by their expectation values (the mean field approximation), one ends up with a set of nonlinear coupled equations.

(1) The Dirac equation with potential terms involving the meson and e.m. fields describing the nucleon dynamics;

(2) A set of Klein-Gordon type equations with sources involving nucleonic currents and densities, for the mesons and photon.

This set of equations, known as RMF equations is to be solved self-consistently.

The pairing correlations, essential for the description of open shell nuclei, can be incorporated either by simple Bardeen-Cooper-Schrieffer (BCS) prescription, or self-consistently through Bogoliubov transformation. The latter procedure leads to the relativistic Hartree Bogoliubov (RHB) equations [9]. The RHB equations have two distinct parts: the self-consistent field (h_D) that describes the long range particle-hole correlations and the pairing field ($\hat{\Delta}$) that accounts for the correlations in the particle-particle (pp) channel. The former involves the nucleon mass M, the scalar field σ and ω^o, ρ_3^o and A^o the Lorentz time like components of the omega, rho mesons and the e.m. fields, respectively. These fields are to be determined self-consistently through the Klein-Gordon equations [9] with sources (nuclear currents and densities) involving superspinors $[U(V)]$. The pairing field $\hat{\Delta}$ is expressed in terms of the matrix elements of the two body nuclear potential V^{pp} in the pp channel and the pairing tensor involving the superspinors (U,V). In the case of the constant gap, $\hat{\Delta}(\equiv\Delta)$ becomes diagonal resulting in the BCS type expressions for the occupation probabilities. As a result, the RHB equations reduce to the RMF equations with a constant gap. A reliable and satisfactory derivation of V^{pp} is not yet achieved in RMF (see Refs. [9,10]). Therefore, in practical calculations, it is customary to adopt a phenomenological approach while solving the RHB equations. As a result, one often uses for V^{pp}, the finite range Gogny-D1S [11,12] interaction, which is known to have the right pairing content. In the case of the constant gap approximation, the required gap parameters are fixed so as to reproduce the corresponding Gogny D1S pairing energies.

A. Details of calculation

The explicit numerical calculations require the following input information:

(1) parameters appearing in the Lagrangian and

(2) V^{pp} or the pairing gap parameters Δ for the calculation of occupancies.

Several sets of these parameters appearing in the Lagrangian are available in the literature [9,13–15]. In the present work, we use one of the recent and the most successful Lagrangian parameter set, NL3 [13]. The equations are solved using the oscillator basis expansion technique. The RHB equations with the Gogny D1S interaction (for pairing) are solved using the spherical oscillator basis. The corresponding results are denoted by RHB(ob). To ascertain the effect of deformation, we have also solved the RMF equations with the constant gap approximation in the deformed oscillator basis with axial symmetry (the corresponding results are denoted by DEF).

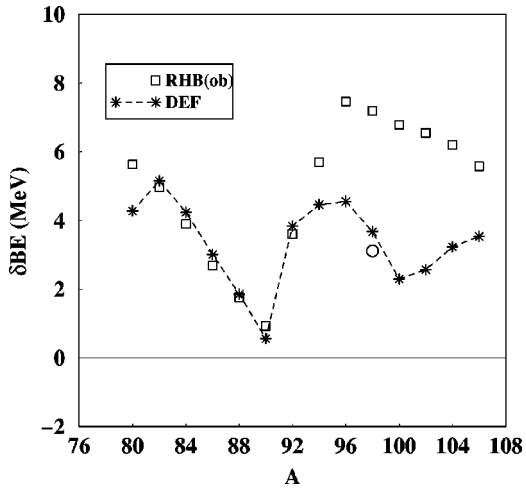

FIG. 1. The difference between the calculated [RHB(ob) and DEF] and the corresponding experimental [16] binding energies for the even Zr isotopes. The open circle indicates the value corresponding to the deepest solution (deeper by just about 0.5 MeV) for ^{98}Zr.

B. Results and discussion

1. Binding energies

The difference between the calculated [RHB(ob) and DEF] and the corresponding experimental binding energies is plotted in Fig. 1 for the various Zr isotopes. Both the calculations agree well (within 1%) with the experiment [16]. At a finer level, however, it is observed that inclusion of deformation does overall improve the agreement between the theory and the experiment. The DEF and the corresponding RHB(ob) results almost coincide for the spherical nuclei $^{82-92}$Zr. Beyond ^{92}Zr, all the isotopes being deformed, the DEF and RHB(ob) results differ. DEF results in this region are found to be closer to the experiment.

2. Quadrupole deformation parameters

The deformation parameter β_2 is extracted from the calculated point neutron (Q_n) and proton (Q_p) quadrupole moments through the relation

$$Q = Q_n + Q_p = \sqrt{\frac{16\pi}{5}}\frac{3}{4\pi}AR_0^2\beta_2$$

with $R_0 = 1.2A^{1/3}$(fm). The calculated quadrupole deformation parameters for the Zr isotopes are plotted in Fig. 2 along with the corresponding Möller-Nix (MN) [17] values. The present calculations are in tune with the MN results. Several Zr isotopes turn out to be prolate while $^{82-90}$Zr are found to be spherical. Except for $^{86-92}$Zr, in almost all the other isotopes, additional nearby solutions are found to exist, hinting towards the possibility of shape coexistence. Interestingly, in the lighter Zr isotopes ($^{78-84}$Zr), all the three solutions (prolate, oblate, and spherical) are found to exist within total

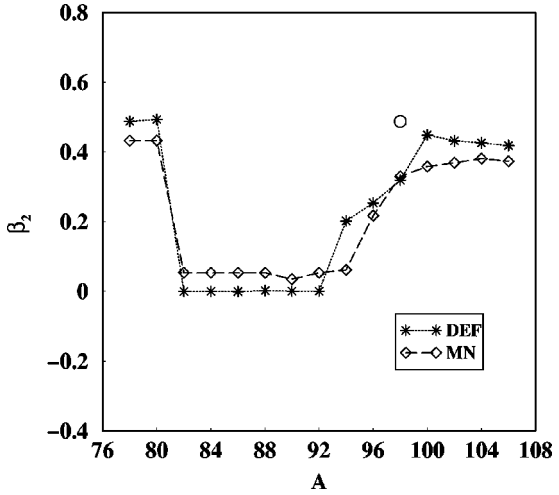

FIG. 2. The calculated (DEF) and the corresponding Möller-Nix (MN) [17] values of the deformation parameters β_2. The open circle indicates the value corresponding to the deepest solution (deeper by just about 0.5 MeV) for ^{98}Zr.

binding energy difference of 1 MeV (2 MeV in the case of ^{78}Zr). On the other hand, in the heavier Zr isotopes (beyond ^{92}Zr) almost degenerate prolate and oblate solutions exist, while only spherical solutions are found to exist beyond ^{106}Zr.

3. Two neutron separation energies

The systematics of the two neutron separation energies gives a fair idea about the shell structure in the nuclei. Thus, the two neutron separation energies (S_{2n}) for the Zr isotopes are now investigated. The calculated [RHB(ob) and DEF] S_{2n} values along with the corresponding experimental values [16] are shown in Fig. 3. The experimental values are reproduced remarkably well by the present calculation. The shell gap at ^{90}Zr is evident. However, it should be noted that theoretically, one gets a larger shell gap in comparison with the experiment. This departure can be rectified through the inclusion of the vector meson self coupling term in the Lagrangian [18]. Beyond the shell closure, the trend in the separation energies is almost flat, indicating the disappearance of shell effects.

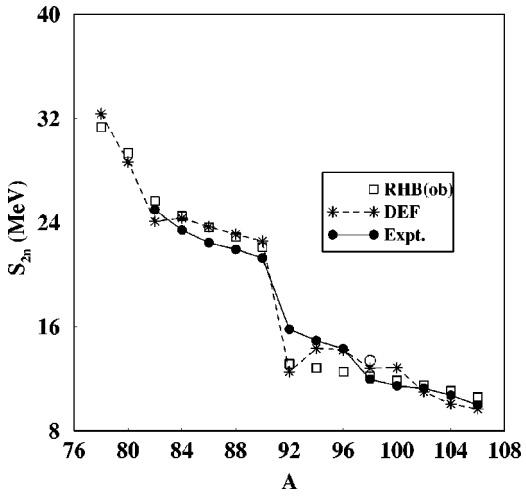

FIG. 3. Two neutron separation energies for Zr isotopes. The results of both the calculations and the corresponding experimental results [16] (where available) are also indicated. The open circle indicates the value corresponding to the deepest solution (deeper by just about 0.5 MeV) for ^{98}Zr. Experimental points are joined by solid lines to guide the eye.

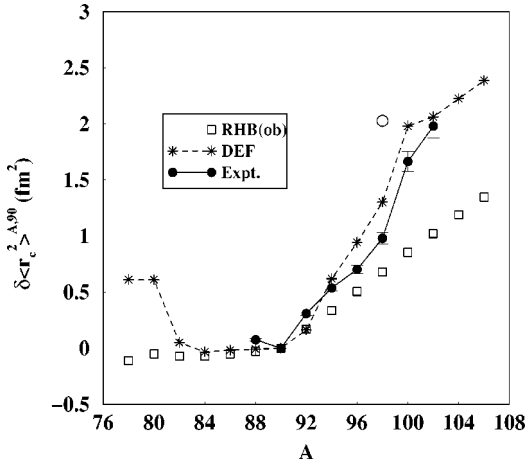

FIG. 4. The calculated [RHB(ob) and DEF] and the corresponding experimental [1] change in the mean square charge radii relative to $N=50$ (^{90}Zr) ($\delta\langle r_c^2\rangle^{A,90}$) for chain of Zr isotopes. The open circle indicates the value corresponding to the deepest solution (deeper by just about 0.5 MeV) for ^{98}Zr. Experimental points are joined by solid lines to guide the eye.

4. Radii

Next we present and discuss the calculated change in the mean square charge radii relative to $N=50$ (^{90}Zr) ($\delta\langle r_c^2\rangle^{A,90}$) for the chain of Zr isotopes. The calculated radii and the corresponding experimental values [1] of $\delta\langle r_c^2\rangle^{A,90}$ for even mass number Zr isotopes are presented in Fig. 4. The graph clearly shows that the DEF results are in good agreement with the experiment. The observed kink at shell closure ^{90}Zr is reproduced. The $\delta\langle r_c^2\rangle^{A,90}$ values in the neutron deficient region $A=82$–$A=90$ remains almost a constant. This observation is in tune with the corresponding experimental values. Another interesting feature is the predicted jump in $\delta\langle r_c^2\rangle^{A,90}$ between ^{82}Zr and ^{80}Zr. Unfortunately, there are no experimental measurements for these nuclei to ascertain this prediction. The anomalous and dramatic jump in the measured $\delta\langle r_c^2\rangle^{A,90}$ values in going from ^{98}Zr to ^{100}Zr is reproduced. It is to be noted that the deepest solution (deeper by just about 0.5 MeV) for ^{98}Zr (indicated by an open circle in the figures) has a slightly larger (by 0.1) prolate deformation. With this solution, the jump in $\delta\langle r_c^2\rangle^{A,90}$ is observed between ^{96}Zr and ^{98}Zr, rather than between ^{98}Zr and ^{100}Zr.

Another interesting and important feature of the loosely bound nuclei is the nuclear skin thickness (defined as difference between the respective rms neutron and proton radii). As more neutrons are added to a nucleus, the corresponding single neutron separation energy decreases. The neutron den-

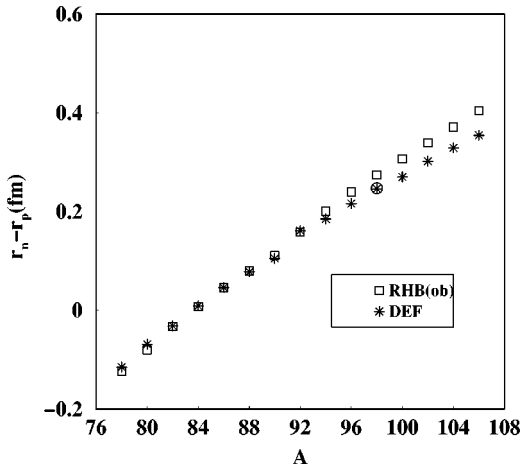

FIG. 5. The calculated nuclear skin thickness for the chain of even Zr isotopes.

sity distribution, therefore, spreads to a larger spatial extent. However, the proton distribution is hardly affected. The difference between the neutron and proton radii thus increases as one moves towards the neutron rich nuclei. The skin thickness, therefore, is a measure of neutron richness or deficiency of the nucleus. The calculated values of the skin thickness are plotted in Fig. 5. The trend discussed earlier is clearly visible from the figure. The skin thickness turns out to be negative for nuclei below ^{84}Zr indicating that the proton density spreads to a larger spatial extent in comparison with the corresponding neutron density while ^{84}Zr is found to have nearly zero skin thickness. Beyond ^{84}Zr, the positive skin thickness is seen to be monotonically increasing with *A*. The DEF and RHB(ob) results are found to be close to each other. They differ slightly in the case of heavier Zr isotopes. As discussed earlier, the calculated DEF charge radii are larger than the corresponding RHB(ob) values in this mass region.

5. Densities

The calculated ($L=0$ projected and renormalized DEF densities) point proton and neutron density distributions for ^{80,82,90,94,98,100}Zr are presented in Fig. 6. In the interior region, all these nuclei are found to have more or less similar proton density distributions. However, in the peripheral region, the proton densities of these nuclei do deviate slightly from each other. For example, the density of ^{80}Zr extends to a somewhat larger spatial extent than that of ^{82}Zr. While the isotopes ^{98}Zr and ^{80}Zr have almost identical proton density distributions, ^{100}Zr differs considerably from the rest. The proton density of ^{94}Zr is found to extend to a lesser extent in comparison with that of ^{80}Zr. The neutron densities, on the other hand, exhibit a different systematics. The densities hardly differ up to ^{90}Zr (shell closure). Beyond ^{90}Zr, the variation in the neutron density is more or less regular. The tail in these cases extends farther with the addition of neutrons.

III. CALCULATION OF OPTICAL POTENTIAL

The folding model is known to be a powerful and successful tool for the analysis of the elastic scattering data. The

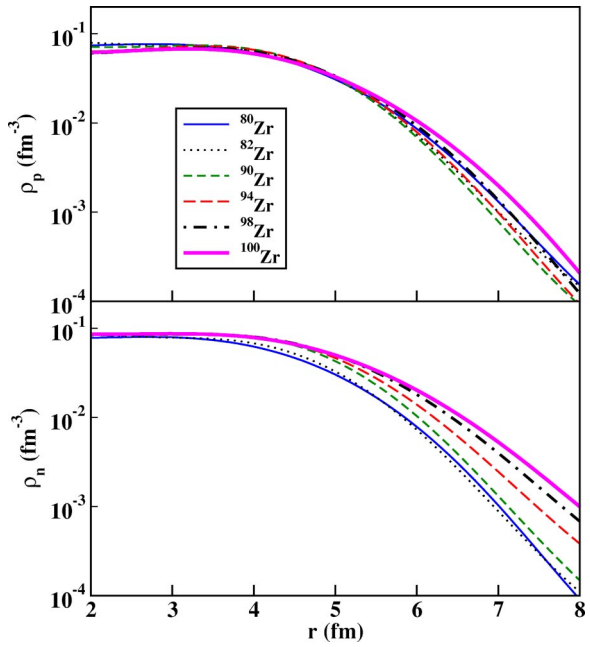

FIG. 6. The calculated ($L=0$ projected and renormalized) DEF densities for selected Zr isotopes.

virtue of the folding model, in general, lies in the fact that it directly links the density profile of the nucleus with the elastic scattering cross section. In this approach, one can determine the nucleon-nucleus optical model potential (OMP) by folding a complex, energy-dependent and density-dependent effective interaction with the nuclear density distributions. Once the parameters of the effective interaction are fixed, the analysis is then sensitive only to the nuclear density distributions. This approach permits probing the differences in matter densities. In the literature a number of successful phenomenological and microscopic optical model approaches have been studied and discussed for proton (neutron)-nucleus scattering. In the phenomenological sector, the most recent successful one is due to Koning and Delaroche [19]. The status of microscopic nucleon-nucleus optical model and its development over the last two decades has been comprehensively covered in a review article by Amos *et al.* [20]. They have developed a microscopic (*g*-folding) prescription which provides complex, nonlocal nucleon-nucleus optical potentials [20,21]. Their prescription employs effective nucleon-nucleon (*NN*) interactions built upon *NN g* matrices and the nucleon-nucleus potentials result from folding these effective interactions with the proton and neutron densities of the target nucleus. Using this approach Amos *et al.* [20] gave predictions of differential cross sections (reaction cross sections) and spin observables which were in good agreement with the data from many nuclei (^{3}He to ^{238}U) and for a wide range of energies (40–300 MeV). Amos *et al.* [20] and Karataglidis *et al.* [22] have shown the expected sensitivity of differential and reaction cross sections to the density distributions in general and the neutron densities in particular. More recently Klug *et al.* [23] have carried out detailed measurement and analysis of 96 MeV neutron scattering from ^{12}C and ^{208}Pb. They have discussed at length, the various phenomenological and microscopic optical model ap-

proaches [7,19–26] employed for the calculation of differential cross sections. In their study of cross section data for ^{12}C and ^{208}Pb, they have concluded that the potentials generated from the various approaches yield cross sections which are in good accord with the data. They have also reported that the results from the procedure of Amos *et al.* [20] yielded the best fits to the data. In the present work, we have employed a semimicroscopic, easy to use optical model prescription due to JLM. This semimicroscopic optical model (MOM) [7] is a Lane-consistent, OMP which is built by folding radial matter densities with an effective interaction in nuclear matter that is based on the extension of the original approach proposed by JLM. This interaction is a hybrid in which the energy and density dependent, spin independent interaction in nuclear matter comes from the original work of JLM [27–30], with a new parameterization defined in Ref. [31]. It may be pointed out that the MOM approach is limited as it does not adequately take into account the important exchange (knock out) amplitudes. The *g*-folding approach of Amos *et al.* incorporates this feature. Consequently, proton scattering data reflect not merely the particle densities but rather the one body density matrices of the structure model. Further, in MOM, the imaginary part of the effective interaction is multiplied [31] by an effective mass as pointed out in Ref. [32]. The JLM interaction, established for nuclear matter, is applied to finite nuclei by using the improved local density approximation and is also extended to deformed nuclei [33,34]. To calculate the complex spin-orbit potential, Scheerbaum's prescription [35] coupled with the phenomenological complex potential depths was used as shown in Ref. [31]. This yields through the standard code MOM [7], the real, imaginary, and spin-orbit parts of the optical potential. The optical potential is then inserted into the optical model code ECIS97 [36] code to get the total reaction and the elastic scattering differential cross sections. Such an analysis of the scattering and the reaction data has been successfully employed in the past [7,37–40]. Here we use this approach for the analysis of the elastic proton scattering on even Zr isotopes.

It is known that the real part of the potential can be determined phenomenologically and microscopically without much ambiguity whereas the imaginary part of the potential is somewhat deficient. Alternatively, one may choose the imaginary part of the OMP phenomenologically to be consistent with the experimental data. Hemalatha *et al.* [41] used the real part of the OMP calculated with MOM code employing the JLM prescription. The imaginary part was chosen phenomenologically for the analysis of 50 MeV proton scattering by a chain of even Zr isotopes. In the present work, the discussion is restricted to microscopic optical model analysis. The real part of the OMP is computed as in Ref. [41]. The calculated real folded potential (with the normalization factor $\lambda_v = 1$) for the stable Zr isotopes, as a function of the radial distance (r), is shown in Fig. 7. These potentials are almost identical to the corresponding real Wood-Saxon part used by Mani *et al.* [5] in their phenomenological analysis of 50 MeV proton scattering from stable Zr isotopes. The phenomenological imaginary part of the Wood-Saxon potential of Ref. [41] and the calculated imaginary part of folded potential for stable Zr isotopes are shown in Fig. 8, plotted as

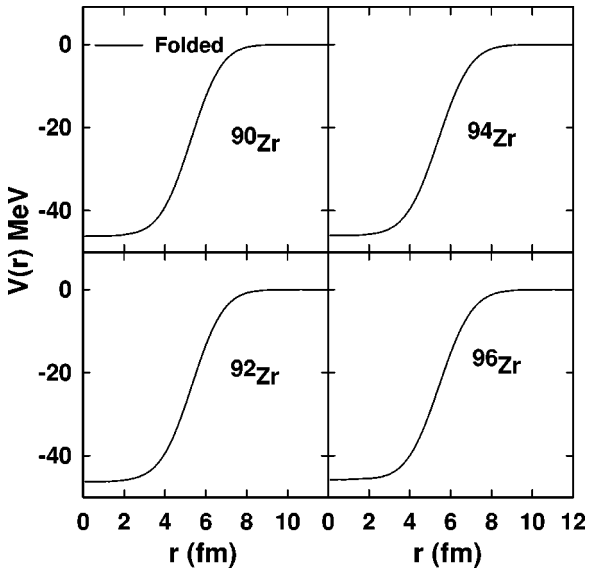

FIG. 7. The real folded potential [$V(r)$] obtained from the MOM calculation.

a function of r. It is evident from the figure that the Wood-Saxon (phenomenological) potential and the corresponding folded potential are quite close to each other at the surface but differ in the interior region. In the present analysis, the spin-orbit part of the potential has been switched off as it has very little influence on the calculated cross sections.

To account for the deficiency in the imaginary part of the OMP, one usually introduces an overall normalization (λ_w) for the imaginary part of the folded OMP to achieve a better agreement between the calculation and the experiment. In the semimicroscopic analysis, the real and imaginary parts of the OMP are replaced by the folded potentials. We have kept the

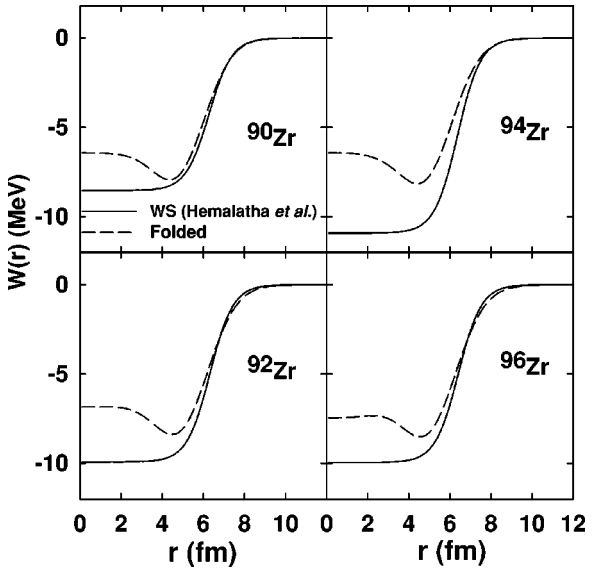

FIG. 8. The imaginary part of the optical potential [$W(r)$] as a function of r for stable Zr isotopes. The solid line is the (phenomenological) Wood-Saxon potential from Hemalatha *et al.* [41] and the dotted line is the folded potential obtained from the MOM calculation.

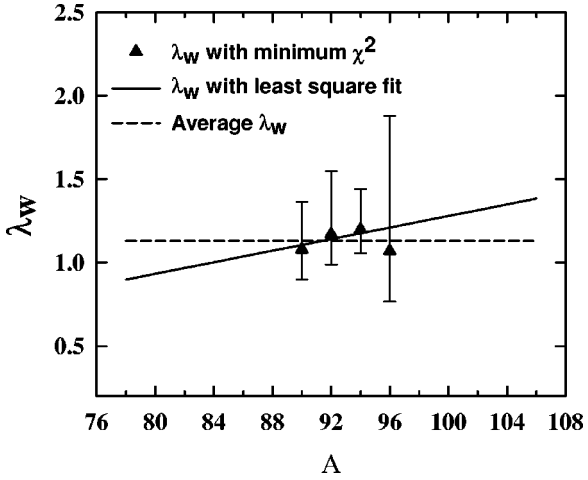

FIG. 9. The variation of normalization factor (λ_w) for the imaginary part of the potential for the chain of Zr isotopes. The filled triangles are the values with minimum χ^2. The solid and the dashed lines are the corresponding values with least squares fit (A dependence) and the average values obtained from the stable Zr isotopes, respectively.

normalization factor $\lambda_v = 1.0$, for the real part of the OMP, throughout. Thus the present analysis has no parameter except λ_w. We have carried out a search on λ_w to achieve a minimum χ^2 in fitting the differential cross-section data for the stable isotopes of Zr. The errors in λ_w have been computed by varying λ_w to get a change in χ^2 by a factor of 2 from the best fit value. The variation of λ_w as a function of A is shown in Fig. 9. It is clear that its value is close to unity and has a mild A dependence. It is expressed as $\lambda_w = 0.017\ A - 0.450$. These λ_w were then used in the code ECIS97 to get the total reaction and differential cross sections for the even isotopes of Zr. For completeness we have also carried out the calculations keeping λ_w as a constant (average value of $\lambda_w = 1.13$ obtained from stable isotopes) for the even Zr isotopes.

IV. CROSS SECTIONS

The experimental and the calculated differential cross sections (using λ_w from the least squares fit), for the elastic scattering of 50 MeV proton incident on $^{88-102}$Zr, are shown in Fig. 10. Clearly the semimicroscopic calculations are in good agreement with the corresponding experimental data. The angular distribution shapes are similar in all the isotopes, however, the magnitudes of the maxima and minima in the angular distribution differ among the Zr isotopes.

The calculated total reaction cross sections (σ_R) using both the sets (average and fitted) of λ_w values for the chain of Zr isotopes are given in Fig. 11. The geometric cross section as per the relation, $\sigma_R = \pi r_0^2 (A_p^{1/3} + A_T^{1/3})^2$ where A_p and A_T are the mass of the projectile (p) and Zr targets respectively, and $r_0 = 1.4$ fm, is also included in the same figure. Clearly, there is a deviation of σ_R from the simple geometric model prediction. The errors on σ_R (shown in Fig. 11) are calculated by a similar procedure as that adopted for λ_w. It is observed that there is a pronounced rise in σ_R in the

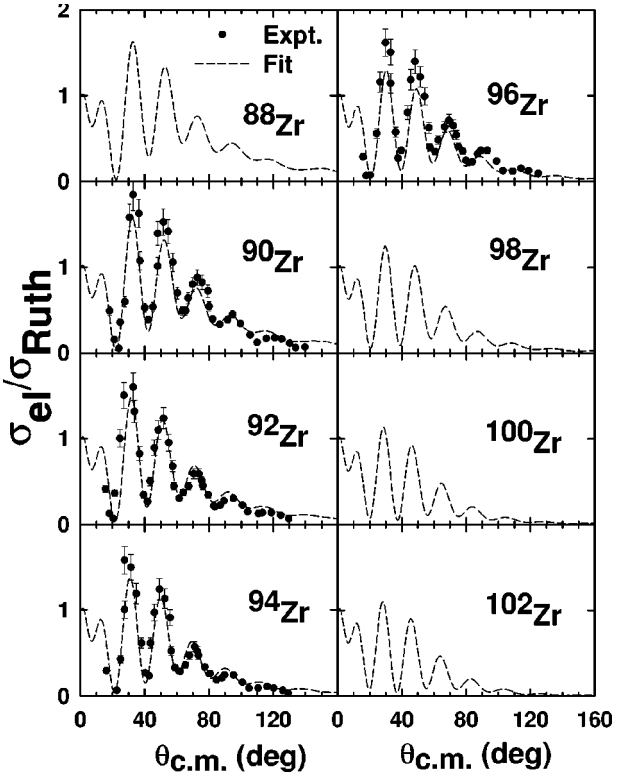

FIG. 10. The ratio to Rutherford cross section for 50 MeV proton scattering from the even isotopes of Zr. The dots are the experimental values taken from Ref. [5] while the dashed line corresponds to the calculation with the least squares fitted λ_w values.

neutron rich region for both sets of λ_w. In both the cases, there is a rise in σ_R in going from $A = 80$ to $A = 82$ and then a sudden fall from $A = 82$ to $A = 84$. There is a monotonic increase in σ_R from $A = 84$ until $A = 106$ with the hint of a slight

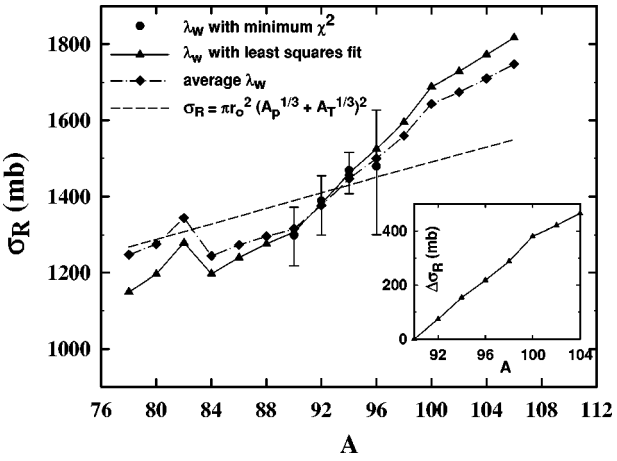

FIG. 11. The total reaction cross section (σ_R) obtained from our analyses of elastic scattering from the chain of even Zr isotopes. The dots with error bars correspond to λ_w values with minimum χ^2. The solid and the dot-dashed lines correspond to the values of λ_w with least squares fit (A dependent) and average ($\lambda_w = 1.13$) values. The variation of the geometric σ_R with A is represented by the dashed line. The inset shows $\Delta\sigma_R^{A,90}$, the difference in σ_R for the chain of even Zr isotopes relative to ^{90}Zr.

jump from $A=98$ to $A=100$. In order to bring out this effect more clearly and be consistent with $\delta\langle r_c^2\rangle^{A,90}$, we have plotted $\Delta\sigma_R^{A,90}$, the difference in σ_R for the chain of Zr isotopes relative to ^{90}Zr. The variation of $\Delta\sigma_R^{A,90}$ with A is shown as an inset in Fig. 11. From the inset, the jump in $\Delta\sigma_R^{A,90}$ from $A=98$ to $A=100$ is evident and is consistent with that of $\delta\langle r_c^2\rangle^{A,90}$ systematics. The experimental value of reaction cross section for 50 MeV protons interacting with ^{90}Zr was measured to be 1214 ± 59 by Menet *et al.* [42]. This is consistent with the value deduced from the fit (as given in Fig. 11) to the differential cross section data.

V. CONCLUSION

The ground state properties such as binding energies, quadrupole deformation parameter, one and two neutron separation energies, neutron and charge radii, etc., have been calculated in the RMF framework for a number of Zr isotopes with $A=78$–106. The calculations are found to be in good accord with the experiment (where available). The deviation of mean square charge radii from the conventional $r_0A^{1/3}$ relation, termed as an anomalous behavior, is reproduced well by the RMF calculations. The calculated RMF densities are folded with the extended JLM, energy, and density dependent nucleon-nucleon interaction to yield the optical potential which in turn is used in the ECIS97 code to get the differential and the reaction cross sections for 50 MeV proton scattering by a chain of even mass number Zr isotopes. The differential cross sections obtained from the semimicroscopic calculations agree remarkably well with the corresponding experimental values. As expected, a definite correlation is observed between the variation of $\delta\langle r_c^2\rangle^{A,90}$ with mass number and the corresponding behavior of the reaction cross section with A. The calculation reveals a kink in the reaction cross section (σ_R) at $A=82$. It is interesting to note that while σ_R values are significantly larger than the geometrical predictions for neutron rich Zr isotopes, they are suppressed for the neutron deficient Zr isotopes for A up to 84. There is a hint of a slight jump in the microscopically calculated σ_R between ^{98}Zr and ^{100}Zr which is in tune with the corresponding sudden jump observed in the rms charge radii. We have also predicted a larger reaction cross section for ^{82}Zr when compared to the values for ^{80}Zr and ^{84}Zr. Experimental verification of the prediction of cross sections for the neutron rich and proton rich Zr isotopes, with the existing RIB facilities, would be interesting.

ACKNOWLEDGMENTS

One of the authors (M.H.) acknowledges the Department of Atomic Energy (DAE) of the Government of India. Partial financial support to Y.K.G. from the BRNS, DAE, Government of India (Proj. No. 2001/37/13/BRNS/692) is gratefully acknowledged.

[1] P. Campbell *et al.*, Phys. Rev. Lett. **89**, 082501 (2002).
[2] E. W. Otten, in *Treatise on Heavy Ion Science*, edited by D. A. Bromley (Plenum Press, New York, 1989), Vol. 8, p. 517, and references cited therein.
[3] E. G. Nadjakov, K. P. Marinova, and Yu. P. Gangrsky, At. Data Nucl. Data Tables **56**, 133 (1994).
[4] I. Tanihata, H. Hamagaki, O. Hashimoto, Y. Shida, N. Yoshikawa, K. Sugimoto, O. Yamakawa, T. Kobayashi, and N. Takahashi, Phys. Rev. Lett. **55**, 2676 (1985).
[5] G. S. Mani, D. T. Jones, and D. Jacques, Nucl. Phys. **A165**, 384 (1971).
[6] Y. K. Gambhir, P. Ring, and A. Thimet, Ann. Phys. (N.Y.), **198**, 132 (1990), and references cited therein.
[7] E. Bauge, J. P. Delaroche, and M. Girod, Phys. Rev. C **63**, 024607 (2001).
[8] J. D. Walecka, Ann. Phys. (N.Y.) **83**, 491 (1974).
[9] P. Ring, Prog. Part. Nucl. Phys. **37**, 193 (1996), and references cited therein.
[10] H. Kucharek and P. Ring, Z. Phys. A **339**, 23 (1991).
[11] J. F. Berger, M. Girod, and D. Gogny, Nucl. Phys. **A428**, 32 (1984).
[12] T. Gonzalez-Llarena, J. L. Egido, G. A. Lalazissis, and P. Ring, Phys. Lett. B **379**, 13 (1996).
[13] G. A. Lalazissis, J. König, and P. Ring, Phys. Rev. C **55**, 540 (1997).
[14] P. G. Reinhardt, M. Rufa, J. A. Maruhn, W. Greiner, and J. Friedrich, Z. Phys. A **323**, 13 (1986); P. G. Reinhardt, Rep. Prog. Phys. **52**, 439 (1989).
[15] M. M. Sharma, M. A. Nagarajan, and P. Ring, Phys. Lett. B **312**, 377 (1993).
[16] G. Audi and A. H. Wapstra, Nucl. Phys. **A565**, 1 (1993); **A565**, 66 (1993).
[17] P. Möller, J. R. Nix, W. D. Myers, and W. J. Swiatecki, At. Data Nucl. Data Tables **59**, 185 (1995).
[18] M. M. Sharma, A. R. Farhan, and S. Mythili, Phys. Rev. C **61**, 054306 (2000).
[19] A. J. Koning and J. P. Delaroche, Nucl. Phys. **A713**, 231 (2003).
[20] K. Amos, P. J. Dortmans, H. V. von Geramb, S. Karataglidis, and J. Raynal, Adv. Nucl. Phys. **25**, 275 (2000), and references cited therein.
[21] K. Amos, S. Karataglidis, and P. K. Deb, Phys. Rev. C **65**, 064618 (2002).
[22] S. Karataglidis, K. Amos, B. A. Brown, and P. K. Deb, Phys. Rev. C **65**, 044306 (2002).
[23] J. Klug *et al.*, Phys. Rev. C **67**, 031601 (2003); **68**, 064605 (2003).
[24] R. Kozack and D. G. Madland, Nucl. Phys. **A509**, 664 (1990).
[25] P. Romain and J. P. Delaroche, in *Proceedings of a Specialists Meeting*, edited by P. Nagel (OECD, Paris, 1997), p. 167, see http://db.nea.fr/html/science/om200/
[26] R. Crespo, R. C. Johnson, and J. A. Tostevin, Phys. Rev. C **46**, 279 (1992).
[27] J. P. Jeukenne, A. Lejeune, and C. Mahaux, Phys. Rev. C **10**, 1391 (1974).
[28] J. P. Jeukenne, A. Lejeune, and C. Mahaux, Phys. Rep., Phys.

Lett. **25**, 83 (1976).
[29] J. P. Jeukenne, A. Lejeune, and C. Mahaux, Phys. Rev. C **15**, 10 (1977).
[30] J. P. Jeukenne, A. Lejeune, and C. Mahaux, Phys. Rev. C **16**, 80 (1977).
[31] E. Bauge, J. P. Delaroche, and M. Girod, Phys. Rev. C **58**, 1118 (1998).
[32] J. W. Negele and K. Yazaki, Phys. Rev. Lett. **47**, 71 (1981).
[33] A. Hogenbirk, H. P. Blok, M. G. E. Brand, A. G. M. van Hees, J. F. A. van Hienen, and F. A. Jansen, Nucl. Phys. **A516**, 205 (1990).
[34] M. Pignanelli, A. Micheletti, R. De Leo, S. Brandenburg, and M. N. Harakeh, Phys. Rev. C **33**, 40 (1986).
[35] R. R. Scheerbaum, Nucl. Phys. **A257**, 77 (1976).
[36] J. Raynal, CEA Report No. CEA-N-2772 (1994).
[37] F. Maréchal *et al.*, Phys. Rev. C **60**, 034615 (1999).
[38] H. Sheit *et al.*, Phys. Rev. C **63** 014604 (2000).
[39] E. Khan *et al.*, Nucl. Phys. **A694**, 103 (2001).
[40] E. Bauge, J. P. Delaroche, M. Girod, G. Haouat, J. Lachkar, Y. Patin, J. Sigaud, and J. Chardine, Phys. Rev. C **61**, 034306 (2000).
[41] M. Hemalatha, A. Bhagwat, A. Shrivastava, S. Kailas, and Y. K. Gambhir, Proceedings of the DAE-BRNS Nuclear Physics Symposium, Mumbai **B46**, 306 (2003).
[42] J. J. H. Menet, E. E. Gross, J. J. Malanify, and A. Zucker, Phys. Rev. C **4**, 1114 (1971).